Natural Variation in Arabidopsis Cvi-0 Accession Uncovers Regulation of Guard Cell CO_2 Signaling by MPK12

Short title: Guard Cell CO2 Signaling

Liina Jakobson[a,*], Lauri Vaahtera[b,*], Kadri Tõldsepp[a*], Maris Nuhkat[a], Cun Wang[c], Yuh-Shuh Wang[a], Hanna Hõrak[a], Ervin Valk[a], Priit Pechter[a], Yana Sindarovska[a], Jing Tang[d] , Chuanlei Xiao[d], Yang Xu[d], Ulvi Gerst Talas[e], Maido Remm[e], Saijaliisa Kangasjärvi[f], M. Rob G. Roelfsema[g], Honghong Hu[d], Jaakko Kangasjärvi [b,h], Mart Loog[a], Julian I. Schroeder[c], Hannes Kollist[a,1], and Mikael Brosché[a,b,1]

[a] Institute of Technology, University of Tartu, Nooruse 1, Tartu 50411, Estonia

[b] Division of Plant Biology, Department of Biosciences, Viikki Plant Science Centre, University of Helsinki, PO Box 65, FI-00014 Helsinki, Finland

[c] Division of Biological Sciences, Cell and Developmental Biology Section, University of California San Diego, La Jolla, CA 92093-0116, USA

[d] College of Life Science and Technology, Huazhong Agricultural University, No. 1 Shizishan street, Hongshan District, Wuhan, 430070, China

[e] Department of Bioinformatics, Institute of Molecular and Cell Biology, University of Tartu, Tartu, 51010, Estonia

[f] Molecular Plant Biology, Department of Biochemistry, University of Turku, FI-20014 Turku, Finland

[g] Molecular Plant Physiology and Biophysics, Julius-von-Sachs Institute for Biosciences, Biocenter, University of Würzburg, Julius-von-Sachs-Platz 2, D-97082 Würzburg, Germany

[h] Distinguished Scientist Fellowship Program, College of Science, King Saud University, Riyadh, Saudi Arabia

* Shared first authors

[1] To whom correspondence may be addressed. E-mail: hannes.kollist@ut.ee or mikael.brosche@helsinki.fi

Mikael Brosché, Division of Plant Biology, Department of Biosciences, University of Helsinki, PO Box 65, FI-00014 Helsinki, Finland. Telephone +358294159436

Hannes Kollist, Institute of Technology, University of Tartu, Nooruse 1, Tartu 50411, Estonia. Telephone +37256470471

Abstract

Plant gas exchange is regulated by guard cells that form stomatal pores. Stomatal adjustments are crucial for plant survival; they regulate uptake of CO_2 for photosynthesis, loss of water and entrance of air pollutants such as ozone. We mapped ozone hypersensitivity, more open stomata and stomatal CO_2-insensitivity phenotypes of the *Arabidopsis thaliana* accession Cvi-0 to a single amino acid substitution in MAP kinase 12 (MPK12). In parallel we showed that stomatal CO_2-insensitivity phenotypes of a mutant *cis* (*C*O_2-*i*nsensitive) were caused by a deletion of MPK12. Lack of MPK12 impaired bicarbonate-induced activation of S-type anion channels. We demonstrated that MPK12 interacted with the protein kinase HT1, a central node in guard cell CO_2 signaling, and that MPK12 can function as an inhibitor of HT1. These data provide a new function for plant MPKs as protein kinase inhibitors and suggest a mechanism through which guard cell CO_2 signaling controls plant water management.

Introduction

Human activities have increased the concentrations of CO_2 and harmful air pollutants such as ozone in the troposphere. During the last 200 years, the CO_2 concentration has increased from 280 to 400 ppm, and it is predicted to double relative to the preindustrial level by 2050 [1]. Elevated CO_2 is likely to have complex effects on plant productivity, since CO_2 is not only a driver of climate change, but also the main substrate for photosynthesis. Altered atmospheric chemistry is not limited to CO_2, the concentration of tropospheric ozone has more than doubled within the past 100 years [2]. Ozone is a notorious air pollutant causing severe damages to crops; present day global yield reductions caused by ozone range from 8.5-14% for soybean, 3.9-15% for wheat, and 2.2-5.5% for maize [3]. Both of these gases enter the plant through stomata, small pores on the surfaces of plants, which are formed by pairs of guard cells. Guard cells also regulate plant water balance since plants with more open stomata allow faster water evaporation. Water availability is the most limiting factor for agricultural production and can cause vast decreases in crop yields [4]. Thus plants are constantly facing a dilemma; assimilation of CO_2 requires stomatal opening, but also opens the gates for entrance of harmful air pollutants and leads to excessive water loss. A consequence of increased atmospheric CO_2 concentration can be higher biomass production [5]; but at the same time plants adjust to elevated CO_2 by partial closure of stomata [5, 6] and altered developmental program leading to reduced stomatal number [7]. CO_2-induced stomatal closure reduces water loss, hence it can directly modify plant water use efficiency (WUE) - carbon assimilated through photosynthesis versus water lost through stomata.

Important components of *Arabidopsis thaliana* guard cell CO_2 signaling are carbonic anhydrases (CA1 and CA4) that convert CO_2 to bicarbonate and the protein kinase HT1 (HIGH LEAF TEMPERATURE 1) that has been suggested to function as a negative regulator of CO_2-induced stomatal movements [8, 9]. Ultimately for stomata to close, the signal has to activate protein kinases such as OST1 (OPEN STOMATA1) that in turn activate plasma membrane anion channels, including SLAC1 (SLOW ANION CHANNEL 1) followed by extrusion of ions and water that causes stomatal closure [10-13]. Bicarbonate-induced activation of SLAC1

has been reconstituted in *Xenopus laevis* oocytes [14, 15]. The pathway was shown to consist of RHC1 (RESISTANT TO HIGH CARBON DIOXIDE 1), HT1, OST1 and SLAC1 [14]; while more recently the importance of CA4, aquaporin PIP2;1, OST1 and SLAC1 was demonstrated [15]. Despite that guard cells are perhaps the best characterized single cell signaling system in the plant kingdom, there are still large gaps in our understanding of how CO_2 signaling in guard cells is regulated, and by which mechanism CO_2 might regulate plant water management and WUE [5, 16, 17].

Natural variation among *Arabidopsis* accessions provides a rich genetic resource for addressing plant function and adaptation to diverse environmental conditions. The accession Cvi-0 from Cape Verde Islands is extremely sensitive to ozone treatment, has more open stomata than Col-0 and its stomata CO_2 responses are impaired [18, 19]. A single amino acid change in Cvi-0 MPK12 (MITOGEN-ACTIVATED PROTEIN KINASE 12) was recently shown to affect water use efficiency as well as stomatal size and to impair ABA-induced inhibition of stomatal opening [20]. Together with MPK9, MPK12 regulates stomatal responses to H_2O_2, ABA and extracellular Ca^{2+} [21]. MPK12 also regulates auxin signaling in roots [22].

Here we present the results of quantitative trait loci (QTL) mapping and sequencing of near isogenic lines (NILs) of Cvi-0 ozone sensitivity. In a parallel approach we mapped more open stomata and CO_2-insensitivity phenotypes of a mutant *cis* (*CO₂ insensitive*). A single amino acid change (G53R) in MPK12 and complete deletion of *MPK12* are the causes of more open stomata and altered CO_2 responses of Cvi-0 and *cis*, respectively. In kinase activity assays we show that MPK12 can act as an inhibitor of the HT1 kinase, suggesting a mechanism for regulation of stomatal CO_2 responses.

Results

Mapping of Cvi-0 ozone sensitivity phenotypes

Our initial QTL mapping of ozone sensitivity in Cvi-0 placed the two major contributing loci on the lower ends of chromosomes 2 and 3 [18]. To identify the causative loci related to the extreme ozone sensitivity and more open stomata of Cvi-0, we created a near isogenic line (NIL) termed Col-S (for Col-0 ozone

sensitive) through eight generations of backcrossing of Cvi-0 with Col-0 (Fig 1A, S1A Fig and S1 Video). In parallel, ozone tolerance from Col-0 was introgressed to Cvi-0, by six generations of backcrossing, which generated the ozone tolerant Cvi-T (S1 Video). Using these accessions, NILs and recombinant inbred lines (RILs), we mapped the causative ozone QTLs to a region of 90 kb on chromosome 2 and 17.70-18.18 Mbp on chromosome 3 (S1B Fig). We have previously shown that the QTL on chromosome 2 also controls plant water loss and stomatal function [18], we split both QTLs by backcrossing Col-S with Col-0 and obtained the NILs Col-S2 and Col-S3. Both of these were less sensitive to ozone than Col-S (S1A Fig), indicating that these QTLs act additively to regulate ozone sensitivity. Col-S2 (but not Col-S3) showed much higher day-time stomatal conductance than Col-0 (Fig 1B). The mapping resolution on chromosome 3 was not sufficient to identify the causative gene. Hence, we focused on Col-S2 and its role in stomatal function. Within the 90 kb mapping region on chromosome 2 one gene, At2g46070 encoding a MAP kinase MPK12, shows strong preferential guard cell expression [21]. A single point mutation was found in Cvi-0 *MPK12* leading to a glycine to arginine substitution at position 53 of the protein.

Stomata-related phenotypes of Cvi-0 and *cis* are caused by mutations in *MPK12*

In a parallel project we observed phenotypic discrepancy between different alleles of *cas* (Calcium-sensing receptor [23]). The *cas-2* (GABI-665G12) line had more open stomata and impaired CO_2 responses, whereas this was neither observed in *cas-1* nor in *cas-3* (Fig 1C and S1C Fig). In a backcross with Col-0 the T-DNA insert in *cas-2* was removed, thereby generating the mutant *cis* (*CO_2 insensitive*). Both *cis* and Col-S2 had impaired responses to high CO_2 (800 ppm) leading to longer half-response times, but a residual CO_2 response could still be observed (Fig 1D and S1E Fig).

Mapping and whole genome sequencing of *cis* × C24 populations revealed a complete deletion of the *MPK12* gene and its neighbor *BYPASS2* in *cis* (Fig 1E and S1D Fig). Thus, *cis* was renamed to *mpk12-4.* A second mutant (*gdsl3-1*) from the GABI collection (GABI-492D11) contained an identical deletion of *BYPASS2* and *MPK12* (S2 Fig). We also identified a line with a T-DNA insert in exon 2 of *MPK12* from the SAIL collection (Fig 1E), which was recently named *mpk12-3* [24]. No full-length transcript was found in

115 *mpk12-3* (S3 Fig). SALK T-DNA insertion lines of *MPK12* were previously described as lethal [21, 22];
116 similarly we were unable to retrieve homozygous plants of the same alleles possibly indicating the presence
117 of an additional T-DNA in an essential gene. The new *mpk12* deletion, SAIL insertion and Col-S2 point
118 mutation alleles allowed a detailed characterization of the role of MPK12 in stomatal regulation.

119 Stomatal conductance was higher throughout the day in all three lines: Col-S2, *mpk12-3* and *mpk12-4* (Fig
120 2A), suggesting that the amino acid substitution in Cvi-0 MPK12 leads to loss of function. Furthermore, Col-
121 0 transformed with *MPK12* from Cvi-0 and F1 plants from a cross of Col-S2 and Col-*gl1* showed stomatal
122 conductance similar to Col-0, excluding the option that the G53R substitution in MPK12 would lead to gain
123 of function (S1F-S1G Fig). Increased stomatal conductance may result from an increased number of
124 stomata, larger stomata or more open stomata. However, the stomatal index, length and density did not
125 differ between the lines, indicating that MPK12 regulates a function related to the stomatal aperture (S4
126 Fig). Because of the higher degree of stomatal opening, the instantaneous WUE was decreased for *mpk12-*
127 *3*, *mpk12-4* and Col-S2 (Fig 2B). Altered WUE was previously also seen in *mpk12-1* and a NIL with Cvi-0
128 MPK12 in L*er* [20]. Cvi-0 and Col-S2 were complemented by expression of MPK12 from Col-0 (Fig 2C and
129 2D). Similarly, *mpk12-4* was complemented by expression of Col-0 MPK12 but not by Cvi-0 MPK12 (Fig 2E).
130 We conclude that MPK12 is a crucial regulator of stomatal conductance and a single amino acid
131 substitution (G53R) in Cvi-0 leads to a loss of function in MPK12.

132 **MPK12 functions in guard cell CO_2 signaling**

133 Reduction of CO_2 levels inside the leaf [25] is a signal that indicates shortage of substrate for
134 photosynthesis and triggers stomatal opening. The rate of stomatal opening in response to low CO_2 was
135 severely impaired in *mpk12* and Col-S2 (Fig 3A and S5A Fig). Another signal for stomatal opening is light;
136 this response was intact in *mpk12* (S5B-C Fig). The hormone abscisic acid (ABA) has dual roles in stomatal
137 regulation; it induces stomatal closure, but also inhibits light-induced stomatal opening. The latter response
138 was impaired in *mpk12* and Col-S2 (Fig 3B and S5C Fig). Stomata close in response to several signals
139 including darkness, reduced air humidity, ozone pulse, elevated CO_2 and ABA. Of these, only the response

to elevated CO_2 was impaired in *mpk12* and Col-S2 (Fig 3C, 3D, S5D-H and S6 Fig). CO_2 signaling is impaired in the carbonic anhydrase double mutant *ca1 ca4* [9] and the product of carbonic anhydrase, bicarbonate, activates S-type anion currents [11]. In Col-S2 and *mpk12-4,* bicarbonate-induced S-type anion currents were strongly impaired (Fig 3E). Collectively, these data indicated that MPK12 has an important role in the regulation of CO_2-induced stomatal movements in *Arabidopsis*.

MPK12 interacts with the protein kinase HT1

Only a few regulators of stomatal CO_2 signaling in *Arabidopsis* have been identified. These include the protein kinases HT1 and OST1 [8, 11, 12]. To find the interaction partners of MPK12 we conducted pair-wise split-ubiquitin yeast two-hybrid (Y2H) assays against several kinases and phosphatases involved in stomatal signaling, and against two MPK phosphatases that regulate MPK activity, IBR5 (INDOLE-3-BUTYRIC ACID RESPONSE 5) and MKP2 (MAPK PHOSPHATASE 2) (Fig 4A, 4B and S7A-B Fig). A strong interaction was observed between MPK12 and HT1 in yeast, but not for any of the other kinases or phosphatases except for MPK12 and IBR5. The MPK12-HT1 interaction was also confirmed in *Nicotiana benthamiana* with bimolecular fluorescence complementation (BiFC) (Fig 4C) and split luciferase complementation assay (S7C Fig). Strong interaction between MPK12 and HT1 was observed in the cell periphery (Fig 4C). Recently HT1 was shown to be a plasma membrane associated protein [26]. In contrast, Col-0 and Cvi-0 MPK12-YFP were located inside the cell (S8A-D Fig), hence it is likely that the interaction with HT1 brings MPK12 to the plasma membrane. HT1 interacted with both Col-0 and Cvi-0 version of MPK12, however, HT1 showed weaker interaction with Cvi-0 MPK12 (G53R) both in BiFC and quantitative Y2H assays (Fig 4B and 4C). MPK11, an MPK from the same group as MPK12 [27], did not interact with HT1 (Fig 4C).

IBR5 interacts with MPK12 and regulates auxin signaling in roots [22]. If IBR5 would regulate the activity of MPK12 also in stomatal CO_2 signaling, the *ibr5* mutant would have been expected to display altered CO_2-related stomatal phenotypes. However, *ibr5-1* exhibited wild type stomatal phenotypes in response to CO_2 changes (Fig 3A, 3C, S5A and S5E Fig), indicating that IBR5 does not play a role in the regulation of MPK12 activity in the guard cells.

MPK12 inhibits HT1 activity

The position of MPK12 in ABA and CO_2 signaling was further explored through genetic analysis. The Col-S2 *ht1-2* and *mpk12-4 ht1-2* double mutants had closed stomata similar to *ht1-2* (Fig 4D), suggesting that *HT1* is epistatic to *MPK12*. The strong impairment of stomatal function in *abi1-1* (*ABA insensitive1-1*) was additive to Col-S2 in the double mutant Col-S2 *abi1-1* (Fig 4D). Hence, signaling through MPK12 seems to act, at least to some extent, independently of the core ABA signaling pathway. Taken together, the MPK12-HT1 interaction (Fig 4A-C) and the epistasis between *ht1-2* and *mpk12-4* (Fig 4D) suggest that MPK12 regulates the activity of HT1. To test this directly, we performed *in vitro* kinase assays with casein as the substrate for HT1 (Fig 5A). HT1 displayed strong autophosphorylation and phosphorylated casein efficiently. Addition of the Col-0 version of MPK12 and its hyperactive version (Y122C) effectively inhibited HT1 activity (Fig 5A and quantified in Fig 5B). A point mutated version (K70R) designed to remove the kinase activity of MPK12 also inhibited autophosphorylation activity of HT1 and phosphorylation of casein by HT1, although to a lesser extent (Fig 5B). Importantly, the Cvi-0 version of MPK12 (G53R) displayed strongly suppressed inhibition of HT1 activity (Fig 5A, and 5B). MPK12 did not phosphorylate the kinase dead version of HT1 (K113M) (Fig 5C). Kinase dead HT1 (K113M) was used as substrate, since the strong autophosphorylation activity of HT1 would otherwise have obscured the result. Wild type MPK12 and hyperactive Y122C displayed autophosphorylation, whereas MPK12 (G53R) as well as MPK12 (K70R) had lost the autophosphorylation activity indicating that the G53R substitution in Cvi-0 MPK12 disrupts the kinase activity of the protein (Fig 5C). Modeling of the MPK12 structure supported a major role for G53, since it was located in the glycine rich loop important for binding of ATP (S9 Fig). MPK11 that belongs to the same group as MPK12, was not able to affect HT1 kinase activity indicating specificity for MPK12 in the inhibition of HT1 (S10 Fig).

We conclude that the stomatal phenotypes of *mpk12* mutants and Cvi-0 can be explained by a lack of inhibition of HT1 activity by MPK12, which leads to more open stomata and impaired CO_2 responses (Fig 2A, 3, 5A, 5C and 6).

Evolutionary considerations of MPKs in the regulation of guard cell CO_2 signaling

MPK12 belongs to the same group of MPKs as MPK4, a crucial regulator of pathogen and stress responses [27]. In tobacco, the silencing of MPK4 impaired CO_2-induced stomatal closure [28]. This raises the question whether: (I) MPK4 and MPK12 have a shared function in the regulation of stomatal responses in *Arabidopsis*; or (II) they have specialized function, for example through gene duplication, leading to MPK4 that regulates pathogen responses and MPK12 that regulates stomatal responses to CO_2. If Arabidopsis MPK12 is derived from MPK4 then this should be visible in a phylogenetic analysis. We identified all MPK sequences from representative angiosperm species and performed a phylogenetic analysis (S11 Fig). The gene duplication event giving rise to MPK12 from ancestral MPK4 appeared to be specific to *Brassicaceae*. The Arabidopsis *mpk4* mutant is severely dwarfed preventing accurate stomatal measurements. However, guard cell specific silencing of *MPK4* in *mpk12-4* led to stronger stomatal CO_2 insensitivity (Hõrak et al. submitted), hence in guard cells MPK4 is acting redundantly with MPK12 in stomatal CO_2 signaling. The phylogeny analysis also indicated that *MPK4* was independently duplicated in both grasses and *Solanaceae* (S11 Fig), thus it is likely that in these species several MPKs related to MPK4 may regulate CO_2–induced stomatal responses. However, since MPK11 did not inhibit HT1 activity (S10 Fig), the function of MPKs as kinase inhibitors may be restricted to MPK12 and its closest relatives including MPK4.

Discussion

Natural variation within a species holds great potential to identify regulatory mechanisms that are not easily uncovered through mutant screens. The Cvi-0 accession originates from the Southern border of the *Arabidopsis* distribution area, the Cape Verde Islands. The Ler × Cvi RIL population was one of the first RILs produced and it has been phenotyped for multiple traits [29]. Despite this, only a few QTLs from Cvi-0 have been identified at the molecular level. Our earlier research identified a locus related to ozone sensitivity and more open stomata phenotype of Cvi-0 in chromosome 2 [18]. Recently the G53R substitution in MPK12 that affects plant water use efficiency was identified by using the Ler × Cvi populations, but the biochemical function of MPK12 in stomatal regulation was not further investigated [20]. Here, we

generated NILs by backcrossing Cvi-0 eight times to Col-0 and show that the same natural mutation in Cvi-0 and lack of MPK12 in *cis* are the causes of ozone sensitivity, more open stomata and altered CO_2 responses of *Arabidopsis* plants. Furthermore, we identify a mechanism by which MPK12 regulates the activity of the protein kinase HT1, a negative regulator of CO_2-induced stomatal movements. The regulators of HT1 have remained largely unknown, despite the exceptionally strong CO_2-insensitivity phenotype of plants with impaired HT1 function [8, 11]. Our findings provide the first evidence for the role of MPK12 in guard cell CO_2 signaling and how this relates to plant water management.

The role of MPKs in *Arabidopsis* guard cell signaling has concentrated on MPK9 and MPK12, which are preferentially expressed in guard cells. Plants with point mutations in *MPK9* (*mpk9-1,* L295F) and *MPK12* (*mpk12-1,* T220I) had wild type ABA responses, but *mpk12-1* has decreased WUE [20]. The *mpk9-1, mpk12-1* and *mpk12-2* alleles are TILLING (Targeting Induced Local Lesions in Genomes) lines in Col-*erecta* background and the previously characterized MPK12-Cvi NIL is in L*er* background [20, 21]. Mutations in *ERECTA* modifies transpiration efficiency and stomatal density, which may have influenced some of the previously described *mpk12-1* phenotypes [20, 30]. In contrast, the full knockout alleles described here, *mpk12-3* and *mpk12-4*, are in Col-0 and imply a major function for MPK12 in CO_2 signaling. Additional roles for MPK12 in stomatal responses have been inferred through the use of the double mutant *mpk9-1 mpk12-1* that has impaired stomatal closure responses to ABA and H_2O_2 treatment, and impaired S-type anion channel activation in response to ABA and Ca^{2+} [21]. It is also highly susceptible to *Pseudomonas syringae* infection and impaired in yeast elicitor, chitosan and methyl jasmonate induced stomatal closure [31]. Since the *mpk9 mpk12* double mutant appears to be more severely impaired in abiotic and biotic stomatal responses and S-type anion channel activation than the loss of function MPK12 alleles (Fig 3), it is possible that MPK12 together with MPK9 regulates stomatal aperture in response to various signals. MPK12 also regulates auxin responses in the root [22, 24]. However, beyond the observation that plants with impaired MPK12 are hypersensitive to auxin inhibition of root growth, no details about the targets of MPK12 in roots are known.

HT1 is a negative regulator of CO_2 signaling and the *ht1-2* mutant has more closed stomata displaying constitutive high CO_2 response at ambient CO_2 levels (Fig 4D, [8]). The opposite phenotypes of *mpk12* and *ht1-2* allowed us to use genetic analysis to position MPK12 in the guard cell signaling network. The stomata of *mpk12 ht1-2* were closed, thus positioning MPK12 up-stream of HT1 and possibly as a direct regulator of HT1 (Fig 4D). CO_2 signaling in guard cells is initiated through the production of bicarbonate by carbonic anhydrases and bicarbonate initiates signaling leading to activation of S-type anion channels [9, 11]. In *mpk12*, the bicarbonate-dependent activation of S-type channels was impaired as previously found for the plants with impaired OST1 and SLAC1 (Fig 3E; [11]). The combined evidence from *mpk12* phenotypes, genetic analysis, and measurements of S-type anion currents all pointed towards MPK12 as a crucial regulator of CO_2 signaling acting through HT1. Indeed, HT1 kinase activity was inhibited in the presence of Col-0 MPK12 but not by the Cvi-0 version of MPK12 (Fig 5A). Thus, the inhibitory function of MPK12 was impaired by the G53R amino acid substitution, probably by its weaker interaction with HT1 (Fig 4 and 5A). This explains the similar phenotypes of the NIL Col-S2, *mpk12-3* and *mpk12-4*; they all display lack of inhibition of the negative regulator HT1 leading to higher conductance at ambient CO_2 levels. Further support for the regulatory interplay between HT1 and MPK12 is provided by the isolation of a dominant mutation in *HT1*, *ht1-8D*, which opposite to *ht1-2,* has constitutively more open stomata and is biochemically resistant to inhibition by MPK12 (Hõrak et al. submitted).

Recently two independent studies used *Xenopus laevis* oocytes as a heterologous expression system to reconstitute bicarbonate-induced activation of the SLAC1 anion channel [14, 15]. Tian et al., [14] reported that a MATE-type transporter, RHC1 functions as bicarbonate-sensing component that inactivates HT1 and promotes SLAC1 activation by OST1. More recently it was demonstrated that expression of RHC1 alone was sufficient to activate ion currents in oocytes; these currents were independent of bicarbonate, calling into question the role of RHC1 as a bicarbonate sensor [15]. Furthermore, it was shown that SLAC1 activation can be reconstituted by extracellular bicarbonate in the presence of aquaporin PIP2.1, CA4 and the protein kinases OST1, CPK6 and CPK23 [15]. However, in the guard cell, any proposed CO_2 signaling pathway should

include HT1, since plants with mutations in HT1 completely lack CO_2–induced stomatal responses [8]. We showed that bicarbonate-induced S-type anion currents were strongly impaired in guard cells protoplasts, which lacked functional MPK12 (Fig 3E). Thus, MPK12 and possibly other MPKs that are expressed in guard cells play a role in controlling the activity of HT1 and future research should identify the signaling pathway upstream of MPK12. Dissection of different domains in SLAC1 revealed that the CO_2 signal may involve the transmembrane region of SLAC1, whereas ABA activation of SLAC1 requires intact N- and C-terminus [32]. Hence, ABA and CO_2 regulation of SLAC1 could use different signaling pathways, and this may explain the lack of strong ABA phenotypes in plants carrying mutations in *MPK12*.

Stomata also regulate other aspects of leaf function, for example pathogen entry into leaves. Cvi-0 has altered phenotypes in many traits including drought and pathogen resistance [29, 33, 34]. All of these traits are at least partly regulated through proper stomatal function, thus the MPK12-HT1 regulatory module identified here may influence many of the previously observed phenotypes of Cvi-0. G53 is conserved in all *Arabidopsis* MPKs [20], and is located in the glycine-rich loop that coordinates the gamma-phosphate of ATP. Since the G53 of MPK12 is replaced with the bulky and charged arginine in Cvi-0, it would be expected to impair kinase activity, which was indeed observed (Fig 5C). R53 of Cvi-0 MPK12 is predicted to be positioned at the protein surface, which could explain the weaker interaction with HT1 (Fig 4 and S9 Fig). We propose that negative regulation of stomatal CO_2 signaling by HT1 is alleviated through interaction with MPK12 and MPK4 (Fig 6; Hõrak et al. submitted). The similar impairment of CO_2 signaling and activation of S-type anion channels when MPK4 function is silenced in tobacco [28] and when MPK12 is absent in *Arabidopsis* (Fig 3E), combined with the phylogenetic analysis showing that MPK4 has duplicated also in grasses (S11 Fig) indicate that the MPK12-HT1 CO_2 regulatory module identified here may be broadly conserved throughout angiosperms. Further studies into the mechanisms controlling activation of MPKs in guard cells will help to identify the early events in the perception of altered CO_2 concentrations.

Materials and methods

Plant Material and Growth Conditions. Col-0, Col-*gl*, Cvi-0, *gdsl3-1* (GABI-492D11; CS447183), *cas-1* (SALK_070416), *cas-2* (GABI-665G12) and *cas-3* (SAIL_1157_C10) were from the European Arabidopsis Stock Centre (www.arabidopsis.info). Seeds of *ht1-2* were a gift from Dr. Koh Iba. Col-0 × Cvi-0 RILs were obtained from INRA Versailles. The *abi1-1* allele used was in Col-0 accession. Double mutants and other crosses were made through standard techniques and genotyped with PCR based markers (S1 Table).

For ozone screening, seeds were sown at high density on a 1:1 v/v mixture of vermiculite and peat (type B2, Kekkilä, Finland), and kept for 2 d at 4 °C for stratification. The plants were grown in controlled growth chambers (Bio 1300,Weiss Umwelttechnik, Germany) under a 12 h photoperiod, 23/19 °C day/night temperature and 70/90% relative humidity or growth rooms with equivalent growth conditions. The average photosynthetic photon flux density (PPFD) during the light period was 200 mmol m^{-2} s^{-1}.When seedlings were 1 week old, they were transplanted into 8 × 8 cm pots at a density of five plants per pot.

Three-week-old plants were exposed to ozone in growth chambers under the same conditions as they were grown until the experiments. Ozone exposure was acute (300– 350 ppb for 6 h) and started 2 h after light was switched on. Ozone damage was visualized with trypan blue stain or quantified as electrolyte leakage.

Mapping of Cvi-0 ozone sensitivity QTLs. Near isogenic lines (NILs) were created by crossing Col-0 with Cvi-0 and selecting the most ozone sensitive plant in F2 and backcrossing to Col-0 for eight generations (generating Col-S) or selecting the most tolerant plant and backcrossing to Cvi-0 for six generations (generating Cvi-T). The genomes of Cvi-0 and Col-S were sequenced at BGI Tech Solutions (Hongkong) with Illumina technology and the genomes of Col-S and Cvi-T were sequenced at the DNA Sequencing and Genomics lab, University of Helsinki, with SOLiD technology. The 90 bp long Illumina paired end sequencing library reads were mapped onto the Col-0 reference genome (TAIR10) with using Bowtie2 aligner (version 2.0.0-beta7;[35]) in “end-to-end” alignment mode, yielding an average genomic sequence coverage of 45 fold. Variation calling and haplotype phasing was performed with the help of samtools (Tools for alignments in the SAM format, Version: 0.1.18 ;[36]). Based on the aligned sequences various PCR-based markers (S1 Table) were designed to genotype Cvi-0 versus Col-0 in the NILs and informative RILs from the

315 INRA Versailles Col-0 × Cvi-0 RIL population. The markers were also used to genotype ozone sensitive
316 individuals from segregating F2 populations.

317 **Mapping of *cis* mutation.** Mapping population was created by crossing *cis* (Col-0) and C24 as an *Arabidopsis*
318 genotype with low stomatal conductance. High water loss from excised leaves and decreased responses to
319 high CO_2 were used as a selective trait. Rough mapping with 22 markers using 59 F2 samples showed
320 linkage to the bottom of chromosome 2, at the marker UPSC_2-18415 at 18,4 Mbp. Pooled genomic DNA
321 from 66 selected F3 lines was used for sequencing. Whole genome sequencing was conducted with Illumina
322 HiSeq 2000 and the reads were mapped against Col-0 genome (release TAIR10) by BGI Tech Solutions
323 (Hongkong). For mapping the genomic area of the mutation the Next Generation Mapping (NGM) tool was
324 used [37], which positioned the mutation on chromosome 2 between 18 703 644-19 136 098 bp. The
325 deletion mutation in *cis* was verified by PCR to be 4 770 bp (at the position 18 945 427-18 950 196 bp).

326 **Complementation lines.** *MPK12* and its promoter were amplified from Col-0 or Cvi-0 genomic DNA using
327 Phusion (Thermo Scientific) and Gateway (Invitrogen) cloned into entry vector pDONR-Zeo. Subsequently,
328 the genes were cloned into pGWB13 and pMCD100. Plants were transformed with floral dipping [38].

329 **Southern blotting analyses.** Total DNAs from different genotyping plants were extracted by CTAB method,
330 and 12 micrograms of total DNA was digested by Hind III or EcoRI. The DNAs were running on the gel and
331 transformed onto Nylon membrane. Hybridization was performed with digoxigenin-labeled specific
332 genomic DNA amplified by primers F3 and R4 for 12 h. The membrane was washed several times by
333 washing buffer and Maleic acid buffer. The membrane was blocked by blocking solution for 1 h at room
334 temperature and washed and incubated with anti-DIG-AP for 30 min. Detection was performed using
335 substrate DIG CSPD.

336 **Plant growth and experimental settings for gas-exchange measurements.** Seeds were planted on soil
337 mixture consisting of 2:1 (v:v) peat:vermiculite and grown through a hole in a glass plate covering the pot
338 as described previously (34). Plants were grown in growth chambers (MCA1600, Snijders Scientific,

Drogenbos, Belgium) at 12/12 h day/night cycle, 23°/20° C temperature, 100 µmol m^{-2} s^{-1} light and 70% relative humidity (RH). For gas-exchange experiments, 24-30-day-old plants were used.

Stomatal conductance of intact plants was measured using a rapid-response gas exchange measurement device consisting of eight through-flow whole-rosette cuvettes [39]. Prior to the experiment, plants were acclimated in the measurement cuvettes in ambient CO_2 concentration (~400 ppm), 100 µmol m^{-2} s^{-1} light (if not stated otherwise) and ambient humidity (RH 65-80%) for at least 1 h until stomatal conductance was stable. Thereafter, the following stimuli were applied: decrease/increase in CO_2 concentration, darkness, reduced air humidity, and ozone. CO_2 concentration was decreased to 100 ppm by filtering air through a column of granular potassium hydroxide. In CO_2 enrichment experiments, CO_2 was increased by adding it to the air inlet to achieve a concentration of 800 ppm. Darkness was applied by covering the measurement cuvettes. In blue-light experiments, dark-adapted plants were exposed to blue light (50 µmol m^{-2} s^{-1}) from a LED light source (B42180, Seoul Semiconductor, Ansan, South Korea). The decreased/increased CO_2 concentration, darkness and blue light were applied for 58 minutes. In the long-term elevated CO_2 experiment (Fig 1D and S1E Fig), CO_2 concentration was increased from 400 ppm to 800 ppm for 2.5 hours. To calculate stomatal half-response times, the whole 2.5-hour stomatal response to elevated CO_2 was scaled to a range from 0 to 100% and the time when 50% of stomatal closure had occurred was calculated. Humidity was decreased by a thermostat system to 30-40% RH and stomatal conductance was monitored for another 56 min. In ozone experiments the plants were exposed to 350-450 ppb of ozone for 3 minutes and stomatal conductance was measured for 60 minutes after the start of the exposure.

In ABA-induced stomatal closure experiments, 5 µM ABA solution was applied by spraying as described in [40]. At time point 0, plants were removed from cuvettes and sprayed with either 5 µM ABA solution (5 µM ABA, 0.012% Silwet L-77 (PhytoTechnology Laboratories) and 0.05% ethanol) or control solution (0.012% Silwet L-77 and 0.05% ethanol). Thereafter plants were returned to the cuvettes and stomatal conductance was monitored for 56 minutes.

In ABA-induced inhibition of stomatal opening experiments, plants were acclimated in measurement cuvettes in darkness. At time point 0, plants were removed from cuvettes and sprayed with 2.5 µM ABA solution (2.5 µM ABA, 0.012% Silwet L-77 (PhytoTechnology Laboratories) and 0.05% ethanol) or control solution (0.012% Silwet L-77 and 0.05% ethanol). Thereafter plants were returned to the cuvettes, dark covers were removed and stomatal conductance was monitored in light for 56 minutes.

Prior to the measurement of diurnal pattern of stomatal conductance, plants were pre-incubated in the measurement cuvette at least 12 h in respective light and humidity conditions. Plants were measured in 16-minute intervals. Water Use Efficiency (WUE) was calculated based on the data of diurnal experiments as an average of day-time light period (from 9:00 to 17:00).

CO_2-induced stomatal conductance in S2 Fig. Five-week old healthy plants, growing in a growth chamber with 70% humidity and 16 h light/8 h dark light condition, were used for stomatal conductance analyses at different CO_2 concentrations by a LiCOR-6400XT as previously described (9). Relative stomatal conductance values were normalized relative to the average of ten data points preceding the [CO_2] transitions (400 to 800 or 1000 ppm). The data presented are means of at least 4 leaves per genotype ± SEM.

Stomatal aperture. The *MPK12* deletion mutant *mpk12-4* and wild type plants were grown in a growth chamber at 70% humidity, 75 $\mu mol^{m^{-2}\,s^{-1}}$ light intensity, 21°C, and 16 h light/8 h dark regime. Two-week old leaf epidermal layers of both genotypes were preincubated in opening buffer (10 mM MES, 10 mM KCl, and 50 mM $CaCl_2$ at pH 6.15) for 2 h and individually stomata were imaged and tracked for measurement as before treatment. After that the leaf epidermal layers were incubated with buffers containing 10 µM ABA for 30 min and the individually tracked stomata were imaged. Stomatal apertures were measured by ImageJ software and genotype-blind analyses were used. The data presented are means and SEM n=3 experiments, 30 stomata per experiment and condition.

Stomatal index and density. Plants at the age of 28-30 days were used for stomatal index and density measurements. Rosette leaves of equal size were excised and the abaxial side was covered with the dental

resin (Xantopren M mucosa, Heraeus Kulzer, Germany). Transparent nail varnish was applied onto the dried impressions after the removal of the leaves. The hardened nail varnish imprints were attached onto a microscope glass slide with a transparent tape and imaged under Zeiss SteREO Discovery.V20 stereomicroscope. For quantification an image with the coverage of 0.12 mm^2 was taken from the middle of the leaf, next to the middle vein. In total 81-84 plants per line from 2 independent biological repeats were analysed, one leaf from each plant, one image from each leaf. Stomatal index was calculated with the following formula: SI=Stomatal density/(Density of other epidermal cells + Stomatal density).

Stomatal complex length. For the stomatal complex length measurements plants at the age of 28-35 days were used. Whole leaves were pre-incubated for 4 h abaxial side down in the buffer (10 mM MES, 5 mM KCl, 50 µM $CaCl_2$, pH (with TRIS)) in the light. 4-6 plants per genotype and one leaf per plant were analyzed, altogether 84-126 stomatal complexes per genotype were measured.

Y2H interaction tests. Interactions between MPK12 and selected protein kinases and phosphatases were tested in pairwise split-ubiquitin Y2H assays using the DUALhunter and DUALmembrane 3 kits (Dualsystems Biotech). For bait construction, the coding sequences of *MPK12* were PCR-amplified from total cDNAs from Col-0 and Cvi-0. Other *MPK12* variants with point mutations (K70R, Y122C and D196G+E200A) were created by two-step overlap PCR using the Col-0 *MPK12* as a template. *HT1* was also PCR-amplified from Col-0 cDNA. All *MPK12*s and *HT1* were digested with SfiI and cloned to the corresponding site in pDHB1, containing the Cub-LexA-VP16 fusion. For prey constructs, coding sequences of each selected gene was amplified from total Col-0 cDNAs, digested with SfiI, and cloned into either pPR3-N (*HT1, OST1, BLUS1, IBR5, MKP2, MPK12, MPK12G53R, MPK11*) or pPR3-STE (*SnRK2.2, SnRK3.11, ABI1, ABI2, HAB1, HAB2*), containing a mutated NubG. All primers used are listed in Table S1. The pAI-Alg5 with a native NubI was used as a positive prey control, whereas the pDL2-Alg5 containing NubG served as a negative control.

For pairwise Y2H assays, the yeast strain NMY51 was co-transformed with bait and prey plasmids, and grown on SD-Leu-Trp plates to select for presence of both plasmids. At least 10 colonies from each transformation were pooled and resuspended in water to an OD600 of 0.5 from which 100, 1000, and

10000x serial dilutions were prepared, and spotted on SD-Leu-Trp and SD-Leu-Trp-His-Ade plates. SD-Leu-Trp plates were incubated at 30˚C for 2 d, photographed and used for β-galatosidase overlay assays. SD-Leu-Trp-His-Ade plates were incubated for 2-4 d and photographed. The quantitative β-galactosidase assay was performed with three pools of 10 independent colonies from each pairwise combination using the Yeast β-galactosidase assay kit (Thermo Scientific) by the non-stop quantitative method.

BiFC interaction. Binary constructs containing split YFPs were designed and generated for cloning genes of interest by the ligation independent cloning (LIC) method. First, YFPn (amino acids 1-173 of eYFP), YFPc (amino acids 155-279 of eYFP) and the full-length YFP were amplified by multi-PCR steps to incorporate sequences for LIC method and the HA tag at 5' and 3' end, respectively. The PCR products were digested by EcoRI and cloned into the modified p35S/pCAMBIA1390 at the EcoRI/PmlI site to create 35S:YFPn, and 35S:YFPc in the pCAMBIA1390 vector, respectively.

For subsequent cloning, each gene of interest was amplified by two consecutive PCR reactions: first with gene-specific primers, and later with a pair of universal primers designed specifically for the LIC method. All primers used are listed in Table S1. To prepare vectors for LIC, plasmids of 35S:YFPn and 35S:YFPc were linearized by PmlI digestion, followed by T4 DNA polymerase treatment with dGTP to create 15-16 nucleotide 5'-overhangs. For insert preparation, the final PCR products of target genes were incubated with T4 DNA polymerase in the presence of dCTP to create the complementary overhangs with the vectors. Both vector and insert were mixed at room temperature, and proceeded with *E. coli* transformation after 5 min. The final constructs were sequence verified, and transformed to *Agrobacterium tumefaciens* GV1301 for agro-infiltration experiments.

For the BiFC assays, three different agrobacterial clones each harboring a YFPn fusion, a YFPc fusion, or the gene silencing suppressor P19 were co-infiltrated to the leaves of *Nicotiana benthamiana* at an OD600 of 0.2 for each clone in the infiltration buffer (10mM MES, 10mM $MgCl_2$, 200μM acetosyringone). Images were acquired at 3 dpi with a Zeiss LSM710 confocal microscope. The YFP signals were excited by a 514nm laser, and emission between 518-564 nm was collected. All of the acquisition parameters were kept

identical within each experiment, and only images acquired from the same leaves with multiple infiltration spots were compared.

Split luciferase complementation assay. The *MPK12* cDNA was cloned into a vector containing the N-terminal half of luciferase (nLUC) and *HT1* was cloned into the cLUC. The constructs in the Agrobacterium strain GV3101 were co-infiltrated into *N. benthamiana* leaves with P19 at an OD600 of 0.8. The infiltrated leaves after three days of infiltration were harvested for bioluminescence detection. Images were captured with a CCD camera.

Measurement of S-type anion currents. *Arabidopsis* guard cell protoplasts were isolated as described previously [41]. Guard cell protoplasts were washed twice with washing solution containing 1 mM $MgCl_2$, 1 mM $CaCl_2$, 5 mM MES and 500 mM D-sorbitol (pH 5.6 with Tris). During patch clamp recordings of S-type anion currents, the membrane voltage started at +35 to -145 mV for 7 s with -30 mV decrements and the holding potential was +30 mV. The bath solutions contained 30 mM CsCl, 2 mM $MgCl_2$, 10 mM MES (Tris, pH 5.6), and 1 mM $CaCl_2$, with an osmolality of 485 mmol/kg. The pipette solutions contained 5.86 mM $CaCl_2$, 6.7 mM EGTA, 2 mM $MgCl_2$, 10 mM Hepes-Tris (pH 7.1), and 150 mM CsCl, with an osmolality of 500 mmol/kg. The free calcium concentration was 2 µM. The final osmolalities in both bath and pipette solutions were adjusted with D-sorbitol. Mg-ATP (5 mM) was added to the pipette solution before use. 13.5 mM $CsHCO_3$ (11.5 mM free [HCO_3^-] and 2 mM free [CO_2]) was freshly dissolved in the pipette solution before patch clamp experiments. The concentrations of free bicarbonate and free CO_2 were calculated using the Henderson–Hasselbalch equation (pH = pK1+log [HCO_3^-]/[CO_2]). pK1 = 6.352 was used for the calculation. [HCO_3^-] represents the free bicarbonate concentration and [CO_2] represents the free CO_2 concentration.

Protein expression and purification. For *in vitro* kinase assays, HT1, HT1 K113M, MPK11, MPK12, MPK12 G53R, MPK12 K70R and MPK12 Y122C were cloned into pET28a vector (Novagen, Merck Millipore) using primers listed in S1 Table. Point mutations corresponding to K113M in HT1, K70R in MPK12 and Y122C in MPK12 were created with two-step PCR using primers listed in S1 Table.

6xHis-HT1WT, 6xHis-HT1 K113M, 6xHis-MPK12 WT, 6xHis-MPK12 G53R, 6xHis-MPK12 K70R, 6xHis-MPK12 Y122C and 6xHis-MPK11 WT were expressed in *E. coli* BL21(DE3) cells. A 2 mL aliquot of an overnight culture was transferred to a fresh 1 L 2xYT medium and grown at 37 °C to an absorbance of ~0,6 at OD600. The cultures were chilled to 16 °C and recombinant protein expression was induced by 0.3 mM isopropyl b-D-thiogalactopyranoside for 16 h. The cells were harvested by centrifugation (5000 rpm, 10 min, 4 °C) and stored at -80 °C until use.

All purification procedures were carried out at 4 °C. The cells were resuspended in 30 mL of lysis buffer (50 mM Tris-HCl (pH 7.4), 300 mM NaCl, 5% (v/v) glycerol, 1% (v/v) Triton X-100, 1 mM PMSF, 1 µg/ml aprotinin, 1 µg/ml pepstatin A, 1 µg/ml leupeptin) and lysed using an Emulsiflex C3 Homogenizer. Cell debris was removed by centrifugation at 20 000 rpm for 30 min. The protein-containing supernatant was mixed for 1 h at 4 °C with 0.20 mL of Chelating Sepharose Fast Flow resin (GE Healthcare), charged with 200 mM $NiSO_4$ and pre-equilibrated in the lysis buffer. The protein-resin complex was packed into a column and the beads were washed with 5x10 column volumes (CV) of a wash buffer I (50 mM Tris-HCl (pH 7.4), 600 mM NaCl, 5% (v/v) glycerol, 1% (v/v) Triton X-100), 5x10 CV of a wash buffer II (50 mM Tris-HCl (pH 7.4), 300 mM NaCl, 5% (v/v) glycerol, 0.1% (v/v) NP-40) and 2x10 CV of a wash buffer III (50 mM Tris-HCl (pH 7.4), 150 mM NaCl, 5% (v/v) glycerol, 0.1% (v/v) NP-40). The protein was eluted by incubating the beads for 5 min at room temperature with an imidazole containing elution buffer (50 mM Tris-HCl, 150 mM NaCl, 5% (v/v) glycerol, 0.1% (v/v) NP-40, 300 mM imidazole). MPK12 proteins were concentrated and imidazole was removed by Millipore Amicon Ultra-0.5 Centrifugal Filter Concentrators (NMWL 3000). Glycerol was added to a final concentration of 20% (v/v) and 20 µL aliquots of the eluted protein were snap frozen in liquid nitrogen and stored at -80 °C.

***In vitro* kinase assays.** Protein concentrations were estimated on 10% SDS-polyacrylamide gel using BSA as a standard. HT1 kinase activity assay was performed by incubating constant amount of purified recombinant HT1 and 0-30 µM MPK12 or 0-10 µM MPK11 in a reaction buffer (50 mM Tris-HCl (pH 7.4), 150 mM NaCl, 20 mM MgCl2, 60 mM imidazole, 1 mM DTT, 0.2 mg/ml insulin) at room temperature for 10

min. Then casein (1 mg/ml), 500 µM ATP and 100 µCi/ml 32P-γ-ATP were added and reaction aliquots were taken at 30 min time point. Reactions were stopped by the addition of SDS loading buffer. Proteins were separated on a 10% SDS-polyacrylamide gel and visualized by Coomassie brilliant blue R-250 (Sigma) staining. HT1 activity was determined by autoradiography and quantified by ImageQuant TL Software.

Model of MPK12. Protein structure homology modelling of MPK12 was done with SWISS-MODEL [42] using human MPK7 as a template and visualized with Jmol (http://jmol.sourceforge.net/).

Phylogeny analysis.

Profile hidden Markov model (HMM) of MPKs was built with hmmbuild of HMMR3.1b1 using all 20 Arabidopsis thaliana MPKs' full protein sequences aligned with ClustalW. The protein sequences from other analyzed species was downloaded from Phytozome v10 (proteins, primary transcript only) and searched for MPK HMM with hmmsearch of HMMR3.1b. The full-length protein sequences from all species matching MPK HMM were aligned with Muscle and phylogeny tree was generated using PhyML with following settings: Model=LG, Tree searching operations=best of NNI & SPR, Starting tree=BioNJ, Number of bootstrapped data sets = 1000. Three Cyclin-dependent kinases were included in the analysis as an outgroup. Another phylogram was drawn from the same protein sequences using PASTA with similar results (not shown). The protein sequences from other species were named according to the closest relative found in Arabidopsis thaliana using TAIR BLAST 2.2.8. A FASTA file will all protein sequences is provided as S2 Table.

Statistical analysis. Statistical analyses were performed with Statistica, version 7.1 (StatSoft Inc., Tulsa, OK, USA). All effects were considered significant at $p < 0.05$.

Acknowledgments

Tuomas Puukko provided excellent technical assistance. We thank Aleksia Vaattovaara for assistance with the phylogeny analysis.

References

1. Pachauri RK, Allen M, Barros V, Broome J, Cramer W, Christ R, et al. Climate Change 2014: Synthesis Report. Contribution of Working Groups I, II and III to the Fifth Assessment Report of the Intergovernmental Panel on Climate Change. 2014.

2. Vingarzan R. A review of surface ozone background levels and trends. Atmos Environ. 2004;38(21):3431-42. doi: 10.1016/j.atmosenv.2004.03.030. PubMed PMID: WOS:000221838100006.

3. Avnery S, Mauzerall DL, Liu JF, Horowitz LW. Global crop yield reductions due to surface ozone exposure: 1. Year 2000 crop production losses and economic damage. Atmos Environ. 2011;45(13):2284-96. doi: DOI 10.1016/j.atmosenv.2010.11.045. PubMed PMID: WOS:000289819200014.

4. Boyer JS. Plant Productivity and Environment. Science. 1982;218(4571):443-8. doi: DOI 10.1126/science.218.4571.443. PubMed PMID: WOS:A1982PL85100008.

5. Leakey ADB, Ainsworth EA, Bernacchi CJ, Rogers A, Long SP, Ort DR. Elevated CO2 effects on plant carbon, nitrogen, and water relations: six important lessons from FACE. J Exp Bot. 2009;60(10):2859-76. doi: Doi 10.1093/Jxb/Erp096. PubMed PMID: WOS:000267888400009.

6. Keenan TF, Hollinger DY, Bohrer G, Dragoni D, Munger JW, Schmid HP, et al. Increase in forest water-use efficiency as atmospheric carbon dioxide concentrations rise. Nature. 2013;499(7458):324-+. doi: Doi 10.1038/Nature12291. PubMed PMID: WOS:000321910700033.

7. Engineer CB, Ghassemian M, Anderson JC, Peck SC, Hu HH, Schroeder JI. Carbonic anhydrases, EPF2 and a novel protease mediate CO2 control of stomatal development. Nature. 2014;513(7517):246-+. doi: Doi 10.1038/Nature13452. PubMed PMID: WOS:000341362800053.

8. Hashimoto M, Negi J, Young J, Israelsson M, Schroeder JI, Iba K. Arabidopsis HT1 kinase controls stomatal movements in response to CO2. Nat Cell Biol. 2006;8(4):391-U52. doi: Doi 10.1038/Ncb1387. PubMed PMID: WOS:000236560000018.

534 9. Hu HH, Boisson-Dernier A, Israelsson-Nordstrom M, Bohmer M, Xue SW, Ries A, et al.
535 Carbonic anhydrases are upstream regulators of CO2-controlled stomatal movements in guard cells. Nat
536 Cell Biol. 2010;12(1):87-U234. doi: Doi 10.1038/Ncb2009. PubMed PMID: WOS:000272973800017.
537 10. Vahisalu T, Kollist H, Wang YF, Nishimura N, Chan WY, Valerio G, et al. SLAC1 is required for
538 plant guard cell S-type anion channel function in stomatal signalling. Nature. 2008;452(7186):487-U15. doi:
539 Doi 10.1038/Nature06608. PubMed PMID: WOS:000254341300035.
540 11. Xue SW, Hu HH, Ries A, Merilo E, Kollist H, Schroeder JI. Central functions of bicarbonate in S-
541 type anion channel activation and OST1 protein kinase in CO2 signal transduction in guard cell. Embo J.
542 2011;30(8):1645-58. doi: DOI 10.1038/emboj.2011.68. PubMed PMID: WOS:000290306300022.
543 12. Merilo E, Laanemets K, Hu HH, Xue SW, Jakobson L, Tulva I, et al. PYR/RCAR Receptors
544 Contribute to Ozone-, Reduced Air Humidity-, Darkness-, and CO2-Induced Stomatal Regulation. Plant
545 Physiol. 2013;162(3):1652-68. doi: DOI 10.1104/pp.113.220608. PubMed PMID: WOS:000321325700032.
546 13. Negi J, Matsuda O, Nagasawa T, Oba Y, Takahashi H, Kawai-Yamada M, et al. CO2 regulator
547 SLAC1 and its homologues are essential for anion homeostasis in plant cells. Nature. 2008;452(7186):483-
548 U13. doi: 10.1038/nature06720. PubMed PMID: WOS:000254341300034.
549 14. Tian W, Hou CC, Ren ZJ, Pan YJ, Jia JJ, Zhang HW, et al. A molecular pathway for CO2
550 response in Arabidopsis guard cells. Nat Commun. 2015;6. doi: Artn 6057
551 Doi 10.1038/Ncomms7057. PubMed PMID: WOS:000348830300004.
552 15. Wang C, Hu H, Qin X, Zeise B, Xu D, Rappel WJ, et al. Reconstitution of CO2 regulation of
553 SLAC1 anion channel and function of CO2-permeable PIP2;1 aquaporin as carbonic anhydrase 4 interactor.
554 Plant Cell. 2016. doi: 10.1105/tpc.15.00637. PubMed PMID: 26764375.
555 16. Sun ZY, Jin XF, Albert R, Assmann SM. lMulti-level Modeling of Light-Induced Stomatal
556 Opening Offers New Insights into Its Regulation by Drought. Plos Comput Biol. 2014;10(11). doi: ARTN
557 e1003930
558 DOI 10.1371/journal.pcbi.1003930. PubMed PMID: WOS:000345454400020.

559 17. Kollist H, Nuhkat M, Roelfsema MRG. Closing gaps: linking elements that control stomatal
560 movement. New Phytol. 2014;203(1):44-62. doi: Doi 10.1111/Nph.12832. PubMed PMID:
561 WOS:000336970200009.
562 18. Brosché M, Merilo E, Mayer F, Pechter P, Puzorjova I, Brader G, et al. Natural variation in
563 ozone sensitivity among Arabidopsis thaliana accessions and its relation to stomatal conductance. Plant Cell
564 Environ. 2010;33(6):914-25. doi: DOI 10.1111/j.1365-3040.2010.02116.x. PubMed PMID:
565 WOS:000277712800004.
566 19. Monda K, Negi J, Iio A, Kusumi K, Kojima M, Hashimoto M, et al. Environmental regulation of
567 stomatal response in the Arabidopsis Cvi-0 ecotype. Planta. 2011;234(3):555-63. doi: DOI 10.1007/s00425-
568 011-1424-x. PubMed PMID: WOS:000294349900010.
569 20. Des Marais DL, Auchincloss LC, Sukamtoh E, Mckay JK, Logan T, Richards JH, et al. Variation in
570 MPK12 affects water use efficiency in Arabidopsis and reveals a pleiotropic link between guard cell size and
571 ABA response. P Natl Acad Sci USA. 2014;111(7):2836-41. doi: DOI 10.1073/pnas.1321429111. PubMed
572 PMID: WOS:000331396500085.
573 21. Jammes F, Song C, Shin DJ, Munemasa S, Takeda K, Gu D, et al. MAP kinases MPK9 and
574 MPK12 are preferentially expressed in guard cells and positively regulate ROS-mediated ABA signaling. P
575 Natl Acad Sci USA. 2009;106(48):20520-5. doi: DOI 10.1073/pnas.0907205106. PubMed PMID:
576 WOS:000272254400070.
577 22. Lee JS, Wang S, Sritubtim S, Chen JG, Ellis BE. Arabidopsis mitogen-activated protein kinase
578 MPK12 interacts with the MAPK phosphatase IBR5 and regulates auxin signaling. Plant J. 2009;57(6):975-
579 85. doi: DOI 10.1111/j.1365-313X.2008.03741.x. PubMed PMID: WOS:000264088100002.
580 23. Vainonen JP, Sakuragi Y, Stael S, Tikkanen M, Allahverdiyeva Y, Paakkarinen V, et al. Light
581 regulation of CaS, a novel phosphoprotein in the thylakoid membrane of Arabidopsis thaliana. Febs J.
582 2008;275(8):1767-77. doi: DOI 10.1111/j.1742-4658.2008.06335.x. PubMed PMID:
583 WOS:000254499500016.

584 24. Liu JY, Yang HB, Bao F, Ao K, Zhang XY, Zhang YL, et al. IBR5 Modulates Temperature-
585 Dependent, R Protein CHS3-Mediated Defense Responses in Arabidopsis. Plos Genet. 2015;11(10). PubMed
586 PMID: WOS:000364401600048.
587 25. Hanstein S, de Beer D, Felle HH. Miniaturised carbon dioxide sensor designed for
588 measurements within plant leaves. Sensor Actuat B-Chem. 2001;81(1):107-14. doi: Doi 10.1016/S0925-
589 4005(01)00939-X. PubMed PMID: WOS:000172710900015.
590 26. Hashimoto-Sugimoto M, Negi J, Monda K, Higaki T, Isogai Y, Nakano T, et al. Dominant and
591 recessive mutations in the Raf-like kinase HT1 gene completely disrupt stomatal responses to CO2 in
592 Arabidopsis. J Exp Bot. 2016. doi: 10.1093/jxb/erw134. PubMed PMID: 27034327.
593 27. Andreasson E, Ellis B. Convergence and specificity in the Arabidopsis MAPK nexus. Trends
594 Plant Sci. 2010;15(2):106-13. doi: DOI 10.1016/j.tplants.2009.12.001. PubMed PMID:
595 WOS:000275214100006.
596 28. Marten H, Hyun T, Gomi K, Seo S, Hedrich R, Roelfsema MR. Silencing of NtMPK4 impairs CO-
597 induced stomatal closure, activation of anion channels and cytosolic Casignals in Nicotiana tabacum guard
598 cells. Plant J. 2008;55(4):698-708. doi: 10.1111/j.1365-313X.2008.03542.x. PubMed PMID: 18452588.
599 29. Koornneef M, Alonso-Blanco C, Vreugdenhil D. Naturally occurring genetic variation in
600 Arabidopsis thaliana. Annu Rev Plant Biol. 2004;55:141-72. doi: DOI
601 10.1146/annurev.arplant.55.031903.141605. PubMed PMID: WOS:000222766000007.
602 30. Masle J, Gilmore SR, Farquhar GD. The ERECTA gene regulates plant transpiration efficiency
603 in Arabidopsis. Nature. 2005;436(7052):866-70. doi: 10.1038/nature03835. PubMed PMID: 16007076.
604 31. Lee Y, Kim YJ, Kim MH, Kwak JM. MAPK Cascades in Guard Cell Signal Transduction. Front
605 Plant Sci. 2016;7. PubMed PMID: WOS:000369804600001.
606 32. Yamamoto Y, Negi J, Wang C, Isogai Y, Schroeder JI, Iba K. The Transmembrane Region of
607 Guard Cell SLAC1 Channels Perceives CO2 Signals via an ABA-Independent Pathway in Arabidopsis. Plant
608 Cell. 2016. doi: 10.1105/tpc.15.00583. PubMed PMID: 26764376.

609 33. Bouchabke O, Chang FQ, Simon M, Voisin R, Pelletier G, Durand-Tardif M. Natural Variation
610 in Arabidopsis thaliana as a Tool for Highlighting Differential Drought Responses. Plos One. 2008;3(2). doi:
611 Artn E1705

612 Doi 10.1371/Journal.Pone.0001705. PubMed PMID: WOS:000260586500049.
613 34. Perchepied L, Balague C, Riou C, Claudel-Renard C, Riviere N, Grezes-Besset B, et al. Nitric
614 Oxide Participates in the Complex Interplay of Defense-Related Signaling Pathways Controlling Disease
615 Resistance to Sclerotinia sclerotiorum in Arabidopsis thaliana. Mol Plant Microbe In. 2010;23(7):846-60.
616 doi: Doi 10.1094/Mpmi-23-7-0846. PubMed PMID: WOS:000279002500002.
617 35. Langmead B, Salzberg SL. Fast gapped-read alignment with Bowtie 2. Nature methods.
618 2012;9(4):357-9.
619 36. Li H. A statistical framework for SNP calling, mutation discovery, association mapping and
620 population genetical parameter estimation from sequencing data. Bioinformatics. 2011;27(21):2987-93.
621 37. Austin RS, Vidaurre D, Stamatiou G, Breit R, Provart NJ, Bonetta D, et al. Next-generation
622 mapping of Arabidopsis genes. The Plant Journal. 2011;67(4):715-25.
623 38. Clough SJ, Bent AF. Floral dip: a simplified method for Agrobacterium-mediated
624 transformation of Arabidopsis thaliana. Plant J. 1998;16(6):735-43. PubMed PMID: 10069079.
625 39. Kollist T, Moldau H, Rasulov B, Oja V, Ramma H, Huve K, et al. A novel device detects a rapid
626 ozone-induced transient stomatal closure in intact Arabidopsis and its absence in abi2 mutant. Physiologia
627 Plantarum. 2007;129(4):796-803. doi: DOI 10.1111/j.1399-3054.2006.00851.x. PubMed PMID:
628 WOS:000244944800013.
629 40. Merilo E, Jalakas P, Kollist H, Brosché M. The Role of ABA Recycling and Transporter Proteins
630 in Rapid Stomatal Responses to Reduced Air Humidity, Elevated CO2, and Exogenous ABA. Mol Plant.
631 2015;8(4):657-9. doi: 10.1016/j.molp.2015.01.014. PubMed PMID: WOS:000352306500013.

632 41. Pei Z-M, Kuchitsu K, Ward JM, Schwarz M, Schroeder JI. Differential abscisic acid regulation
633 of guard cell slow anion channels in Arabidopsis wild-type and abi1 and abi2 mutants. The Plant Cell.
634 1997;9(3):409-23.
635 42. Bordoli L, Kiefer F, Arnold K, Benkert P, Battey J, Schwede T. Protein structure homology
636 modeling using SWISS-MODEL workspace. Nat Protoc. 2009;4(1):1-13. doi: 10.1038/nprot.2008.197.
637 PubMed PMID: WOS:000265781800001.

638

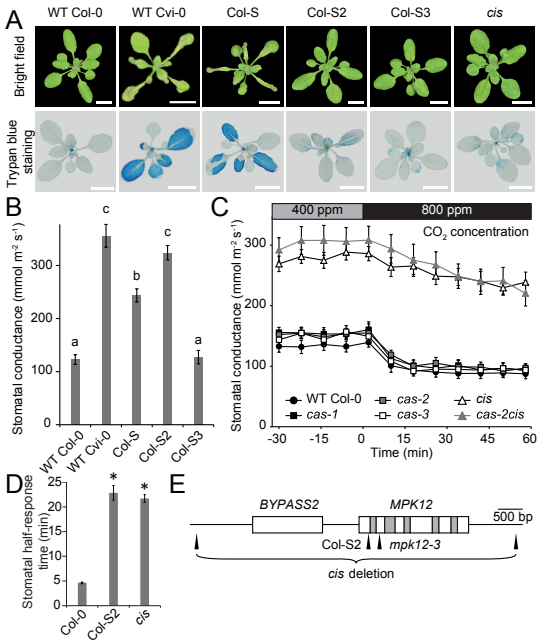

Figure 1.
Mapping of Cvi-0 ozone sensitivity and Cvi-0 and *cis* stomatal responses. (**A**) Tissue damage after 6 h of O_3 exposure (350 ppb). Visual damage of plant rosettes (upper images) and cell death visualized with trypan blue staining (lower images). Scale bar 1 cm. (**B**) Stomatal conductance of Col-0, Cvi-0 and NILs (mean ± SEM, n = 7-12. (**C**) Elevated CO_2 (800 ppm) induced stomatal closure in intact whole plants (n = 9-10, except *cas-2* n = 3. Experiment was repeated at least three times with similar results. (**D**) Stomatal half-response times to elevated CO_2 (800 ppm). Error bars indicate ± SEM (n = 13). Pooled data from two experimental series are shown. **(E)** Gene model of *MPK12* (At2g46070) and *BYPASS2* (AT2g46080). The deletion mutant *cis* (renamed as *mpk12-4*) has a 4772 bp deletion (end and start indicated). Col-S2 has a G to C missense mutation at position 157 of *MPK12*, which leads to G53R substitution in MPK12. The *mpk12-3* mutant has a SAIL T-DNA insertion site in the second exon of *MPK12*. White boxes refer to exons, grey boxes to introns and black line to intergenic regions. Small letters (B) and asterisks (D) denote statistically significant differences according to 1-way ANOVA with Tukey HSD *post hoc* test.

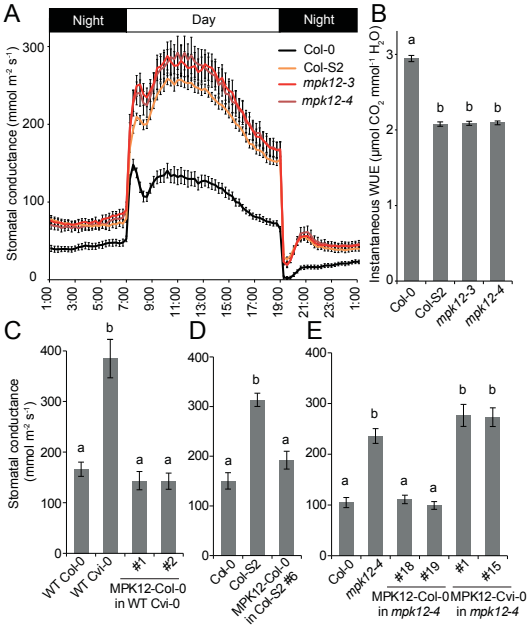

Figure 2.

Stomatal conductance of the NIL Col-S2, *mpk12* mutants and complementation lines.

(**A**) Diurnal pattern of stomatal conductance with 12h/12h light-dark periods (n = 13-16). (**B**) Instantaneous water use efficiency (WUE) measured as an average of day-time light period from 09:00 to 17:00 (n = 3-16). (**C**) Stomatal conductance of Cvi-0 transformed with Col-0 *MPK12* and its promoter in T2 generation (n = 9). (**D**) Stomatal conductance of Col-S2 complementation line in T2 generation transformed with Col-0 *MPK12* and its promoter (n = 5-8). (**E**) Stomatal conductance of T3 transformants in the *mpk12-4* background transformed with either the Col-0 or Cvi-0 version of MPK12 and its respective promoter (n = 5-6). All graphs present mean ± SEM. Small letters denote statistically significant differences according to 1-way ANOVA with Tukey HSD *post hoc* test for either unequal (B, D, E) or equal sample size (C).

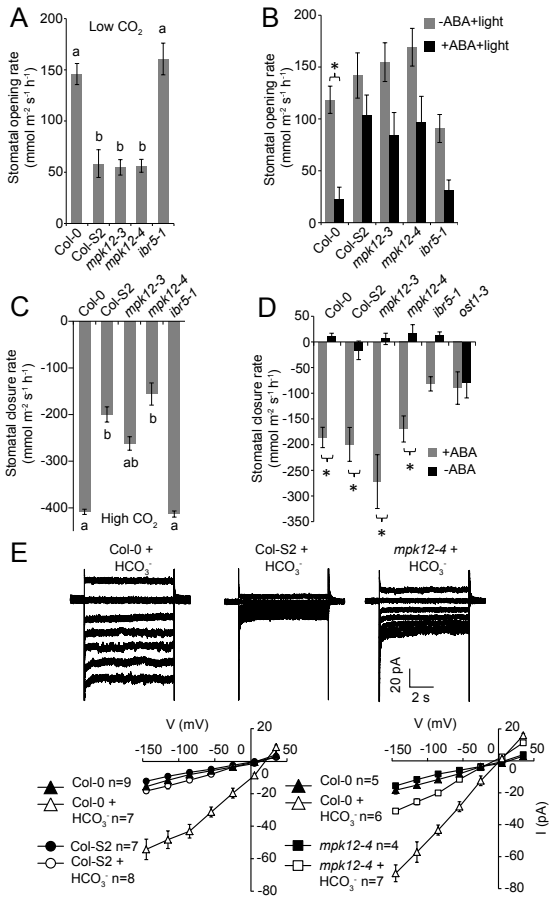

Figure 3.
Stomatal responsiveness of the NIL Col-S2 and *mpk12* mutants to opening and closing stimuli.

(**A**) Stomatal opening rate induced by 100 ppm CO_2 in whole plants (58 min after induction; n = 12-13). (**B**) Light-induced stomatal opening inhibited by 2.5 µM ABA in whole plants (24 min after induction; n = 16-18). (**C**) Stomatal closure rate induced by 800 ppm CO_2 in whole plants (10 min after induction; n = 12-13). (**D**) Stomatal closure rate induced by spraying whole plants with 5 µM ABA solution (24 min after induction; n = 12-14). (**E**) Slow type anion channel activity in guard cell protoplasts treated with HCO_3^- or mock treatment. Small letters (A, C) and asterisks (B, D) indicate statistically significant differences according to 1-way ANOVA and 2-way ANOVA with Tukey HSD unequal N *post hoc* tests ($p < 0.05$), respectively. Error bars mark ± SEM.

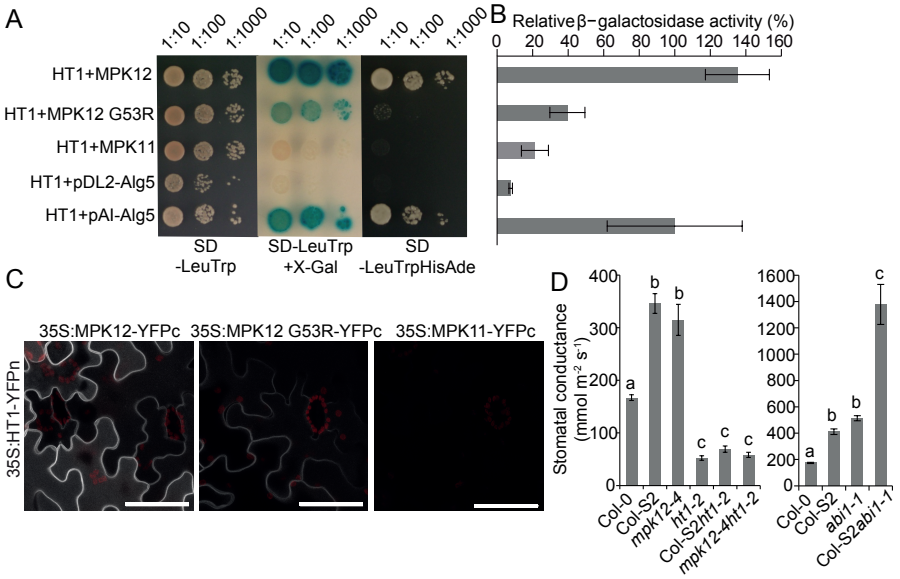

Figure 4.
MPK12 interacts with HT1.

(**A**) Split-ubiquitin yeast two-hybrid assay on the SD-LeuTrp plate (left and middle panels) for the presence of both bait and prey plasmids; X-gal overlay assay (middle) and growth assay on the SD-LeuTrpHisAde plate (right) show HT1 interaction with MPK12, similar to the positive control (pAI-Alg5). Only weak or no interaction was detected with MPK12 G53R or MPK11, similar to the negative control (pDL2-Alg5). (**B**) Quantitative β-galactosidase assay from pools of 10 colonies each. Activities are shown as the percentage of the positive control (± SEM, n = 3). (**C**) BiFC images from the same infiltrated tobacco (*N. benthamiana*) leaf with identical confocal microscopy acquisition settings. Scale bar = 50 µm. (**D**) Steady-state stomatal conductance of Col-S2 *ht1-2*, *mpk12-4 ht1-2* and Col-S2 *abi1-1* double mutants (mean ± SEM, n = 11-13; 1-way ANOVA, Tukey HSD *post hoc* test for unequal sample size). Experiments were repeated at least three times.

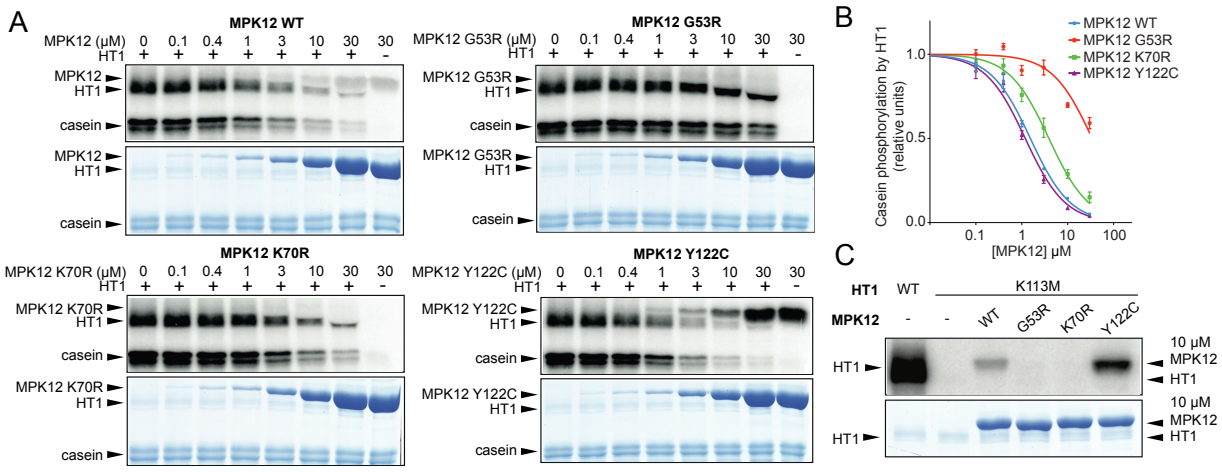

Figure 5.
Regulation of HT1 by MPK12.

(**A**) *In vitro* HT1 kinase activity inhibited by different versions of MPK12 (upper panel: autoradiography of the SDS PAGE gel; lower panel: Coomassie stained SDS PAGE). Reaction mixture was incubated 30 min. (**B**) Casein phosphorylation by HT1 with different MPK12 concentrations (mean ± SEM, n = 3) (**C**) Kinase dead HT1 K113M was not *in vitro* phosphorylated by different versions of MPK12.

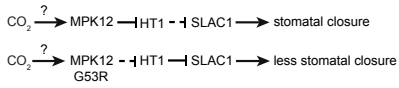

Figure 6.
Schematic representation of guard cell CO_2 signaling pathway via MPK12 and HT1.

The CO_2 signal to stomatal closure is transmitted through MPK12, which inhibits the negative regulator HT1. Cvi-0 MPK12 G53R cannot inhibit HT1.